Biosensors and Bioelectronics 106 (2018) 29–36

Contents lists available at ScienceDirect

Biosensors and Bioelectronics

journal homepage: www.elsevier.com/locate/bios

A sensitive electrochemical nonenzymatic biosensor for the detection of H_2O_2 released from living cells based on ultrathin concave Ag nanosheets

Bo Ma[a], Chuncai Kong[a,b,*], Xuanxuan Hu[a], Ke Liu[c], Qiang Huang[d], Jian Lv[a], Wenjing Lu[a], Xiaojing Zhang[a], Zhimao Yang[a,b], Sen Yang[a,b]

[a] School of Science, MOE Key Laboratory for Non-Equilibrium Synthesis and Modulation of Condensed Matter, State Key Laboratory for Mechanical Behavior of Materials Xi'an Jiaotong University, Xi'an 710049, Shaanxi, China
[b] Collaborative Innovation Center of Suzhou Nano Science and Technology, Xi'an Jiaotong University Suzhou Institute, Suzhou 21500, China
[c] Hubei Key Laboratory of Advanced Textile Materials & Application, College of Materials Science and Engineering, Wuhan Textile University, Wuhan 430200, China
[d] Department of Pediatric Surgery, The Second Affiliated Hospital of Xi'an Jiaotong University, Xi'an, Shannxi 710004, China

ARTICLE INFO

Keywords:
Ag nanosheets
Nonenzymatic biosensor
Hydrogen peroxide
Electrochemical sensor
Living cells

ABSTRACT

Facile synthesis of ultrathin two-dimensional metallic nanosheets with special physical and chemical properties is still challenging. In this work, ultrathin silver nanosheets were synthesized through the galvanic replacement reaction between silver nitrate and Cu microcages without using any surfactant at room temperature. The as-prepared Ag nanosheets (NSs) were concave and had a thickness of sub-10 nm. And the nanosheets exhibited excellent H_2O_2 detection property with a high sensitivity of about 320.3 uA mM^{-1} cm^{-2} and a low detection limit of 0.17 μM in a wide linear range of 5–6000 μM, and a fast response time (less than 2 s). Besides, the real-time detection of H_2O_2 induced from living HeLa and SH-SY5Y cells were also achieved, indicating the potential application of as-prepared Ag NSs in monitoring physiological and dynamic in-clinic pathological processes.

1. Introduction

Hydrogen peroxide (H_2O_2), as one of the most important reactive oxygen species (ROS), is present in various biological tissues (Ferri et al., 1998; Giorgio et al., 2007; Lambeth, 2004; Miller et al., 2005). The concentration of H_2O_2 in cells can be an effective indicator of physiological activities, and an unusual level of H_2O_2 concentration is critical to achieve the trigger diseases, such as neurodegeneration, angiocardiopathy, tumor and so on (Li et al., 2016). Therefore, the accurate and effective detection of H_2O_2 is required to monitor its concentration in living cells and understand the related biological effects. Until now, a large amount of methods have been proposed to detect H_2O_2, including chemiluminescence (Tsaplev, 2012), fluorescence (Liang et al., 2016), photocolorimetry (Chen et al., 2014), colorimetry (Ge et al., 2015) and electrochemical (Bai et al., 2016; Elzanowska et al., 2004). Among these methods, electrochemical detection is considered to be the most prospective technique due to its high sensitivity and fast response, and is divided into enzymatic and nonenzymatic electrochemical detection (Bai and Jiang, 2013; Wang et al., 2013a; Zhou et al., 2014). Traditional enzymatic sensors show great selectivity for H_2O_2. However, their low durability, high cost and conditional sensitivity renders them impractical for commercial applications (Dong et al., 2015). Therefore, a lot of research efforts are devoted to developing low-cost, stable, and robust detection materials, including hydrogels (Jang et al., 2012), noble metals (Jv et al., 2010), nonprecious metals (Wang et al., 2003), redox conducting polymers (Mazeiko et al., 2013), functionalized metal-organic frameworks (Dai et al., 2017) and metal-free carbon-based materials (Guo et al., 2008). As the least expensive noble metals, Ag nanomaterials have been widely used to construct nonenzymatic H_2O_2 sensors due to their highly productive and readily adoptable properties (He et al., 2004). Besides, various morphologies such as Ag nanoparticles (Wang et al., 2013b), nanorods (Shukla et al., 2012), nanobelts (Wang et al., 2012) and nanodendrites (Tajabadi et al., 2015) have been considered advantageous to obtain unique H_2O_2 sensing performance.

Due to the poor electron conduction between adjacent nanoparticles, Ag nanoparticles are still not sensitive enough for nonenzymatic H_2O_2 sensing (Kim et al., 2010). Comparatively speaking, the two-dimensional (2-D) Ag sheets, which exhibit high specific surface favoring the electronic transmission, have attracted significant research attentions (Chhowalla et al., 2013). However, to the best of our knowledge, Ag NSs are mainly synthesized through two methods, one is

* Corresponding author at: School of Science, MOE Key Laboratory for Non-Equilibrium Synthesis and Modulation of Condensed Matter, State Key Laboratory for Mechanical Behavior of Materials Xi'an Jiaotong University, Xi'an 710049, Shaanxi, China.
E-mail address: kongcc@xjtu.edu.cn (C. Kong).

https://doi.org/10.1016/j.bios.2018.01.041
Received 30 October 2017; Received in revised form 6 January 2018; Accepted 18 January 2018
Available online 31 January 2018
0956-5663/

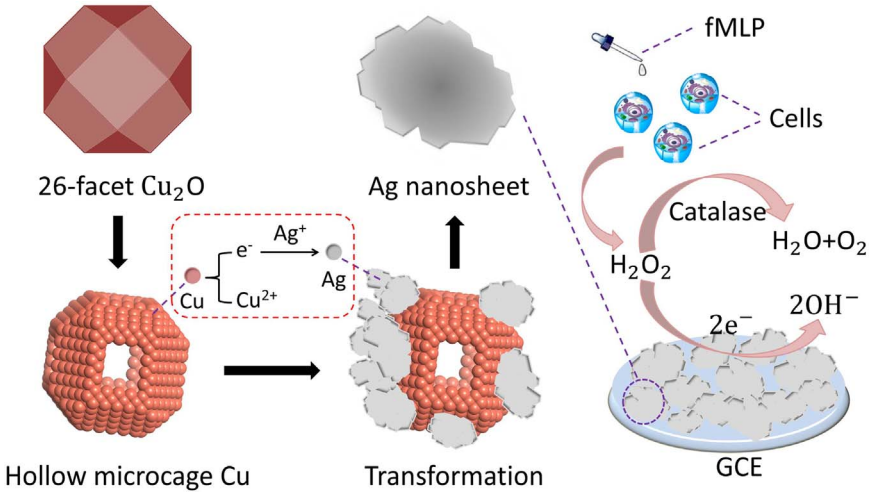

Scheme 1. Schematic illustration of the synthesis of Ag NSs and the modified GCE used for detecting H_2O_2 released from cells by the stimulation of fMLP.

the electrochemical oxidative–reductive approach with the thickness of around tens of nanometers (Lee et al., 2017; Li et al., 2013), while the other one is the galvanic replacement reaction approach with surfactants (PVP and SDS) (Gao et al., 2013; Karimipour et al., 2017). The former method yields product, which is not thin enough for a satisfactory electronic transmission, whereas the latter method has residual surfactant which may reduce the active sites and hinder the detection capability. Little efforts have been made to synthesize sensors consisting of ultrathin Ag NSs. Therefore, there is still a great need to develop a robust synthetic approach for the fabrication of ultrathin Ag NSs.

Herein, we report a facile and common synthesis method for high quality and ultrathin concave Ag NSs with an enhanced electrochemical sensor for the high-sensitivity detection of H_2O_2. The Ag NSs, were formed through a mild (room temperature), galvanic replacement reaction only in the presence of $AgNO_3$ solution and Cu microcages. The monodispersed ultrathin Ag NSs with a thickness of 10 nm exhibited high specific surface area, which can boost their active sites, thus enhancing their electroanalysis performance. The results indicate that this biosensor displays high sensitivity and selectivity toward the reduction of H_2O_2 with a low detected limit of 0.17 μM. By virtue of these merits, the real-time detection of H_2O_2 released from living cells was successfully carried out, indicating the feasibility of Ag NSs as potential H_2O_2 sensing materials.

2. Experimental section

2.1. Synthesis of ultrathin Ag NSs

The typical procedures for the synthesis of 26-facet Cu_2O crystals (Sun et al., 2011) and hollow Cu microcages (Kong et al., 2013) have been reported in our previous works, therefore 26-facets Cu_2O crystals and hollow Cu microcages were firstly synthesized followed previous reports for the further preparation of Ag NSs. Then ultrathin Ag NSs were synthesized as follows: First, 3.2 mg of hollow copper microcages were dispersed in 15 mL deionized water in a conical flask, after the mixture was stirred for 10 min with a rotate speed of 550 rpm. Then, 3.5 mL of $AgNO_3$ aqueous solution (20 mM) was added into the above solution. 2 min later, 1 mL of HNO_3 aqueous solution (20 mM) was added fast. The reaction was kept stirring for 30 min at a room temperature and the mixture turned turbid with a gray color. And then, the obtained was washed thrice with deionized water and ethanol by repeated centrifugation at 7000 rpm for 2 min. Finally, the ultrathin Ag NSs were obtained.

2.2. Construction of the modified electrode and electrochemical measurements

Firstly, the glassy carbon electrode (GCE) (Φ = 5 mm), which was used as working electrode, was polished with 0.5 μm and 50 nm an alumina powder in the aqueous slurry, and then followed by sonication in double distilled water and ethanol solution successively. Before using, the electrode was dried in nitrogen (N_2). Afterwards, the surface of the polished GCE was dropped with a 10 μL aqueous solution of Ag NSs (1 mg/mL). 2 h later, a 10 μL aqueous solution of Nafion (0.05 wt%) was dropped again. Then let it dry at the room temperature. Therefore, Ag NSs-modified GCE was obtained, referred to as Ag NSs/GCE. Including amperometric and cyclic voltammetry (CV), all electrochemical measurements experiments were carried out by a electrochemical analyzer in a conventional three-electrode electrochemical cell, which employs a twisted platinum wire as the counter electrode, an Ag/AgCl (in a saturated KCl solution) as the reference electrode and a Ag NSs/GCE as the working electrode, respectively. In addition, all experiments were carried out in a water bath at room temperature. Prior to the experiment, high-purity N_2 was used to purge the PBS solution for at least 30 min. Moreover, N_2 atmosphere and a mild stir (100 rpm) were maintained during all the amperometric tests.

2.3. Measuring the H_2O_2 released from cancer cells

All the cells were grown in 5% CO_2 in different 75 cm^2 flasks, with in a cell culture medium at 37 °C. After growing to ~ 90% confluence, the cells were collected by centrifugation and washed with PBS three times. A hemocytometer was used to count the number of cells (5×10^6). The packed cells were dispersed in 50 mL of PBS to measure the current response for H_2O_2 detection. 0.5 μM fMLP which could make the cells release H_2O_2 was added as a stimulant. As a comparison, the fMLP was injected into the PBS without cells and with catalase (20 μL, 10–40 K units/mg), respectively.

3. Results and discussion

3.1. Characterization of the prepared ultrathin concave Ag NSs

In order to describe the typical synthetic routes for Ag NSs, the growth and detection progresses were illustrated (as shown in Scheme 1). Additionally, more SEM observations are shown in Fig. S1. At first, the raw material was pure 26-facet Cu_2O having a smooth surface (as shown in Fig. S1a). Then, the monodispersed Cu particles were loaded in-situ on the surface of (1 1 1) and (1 1 0) facets of Cu_2O. When the time gradually increased to 120 min, the Cu_2O core was fully consumed

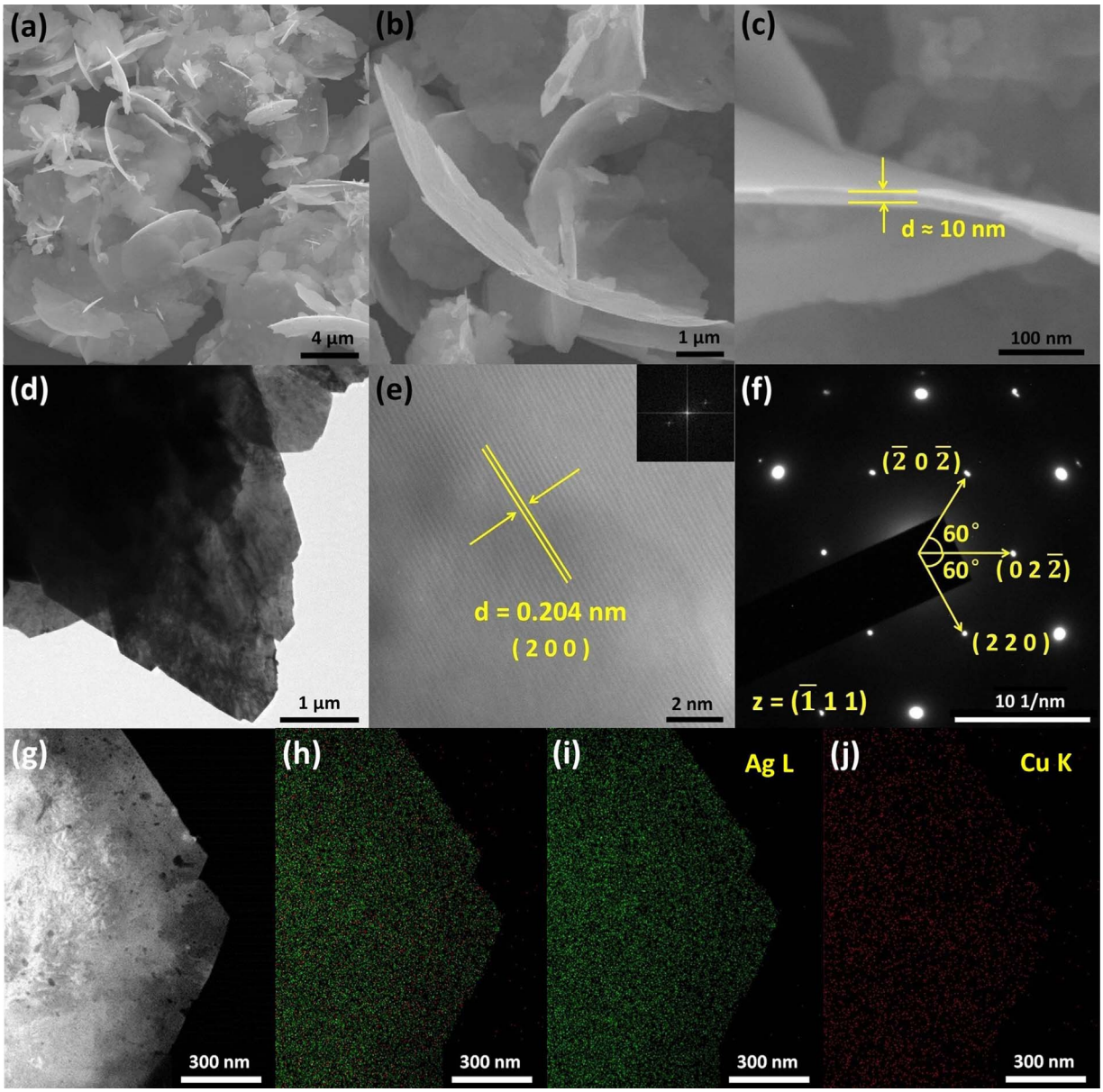

Fig. 1. (a) and (b) Low-magnification FESEM image of Ag NSs. (c) High-magnification FESEM images of an individual Ag nanosheet. (d) Low-magnification, (e) HRTEM TEM images and (f) SAED pattern of Ag NSs. (g) HAADF-STEM image of Ag NSs. (h-j) Corresponding EDS mapping images, green color represents Ag and red color represents Cu in the EDS maps.(For interpretation of the references to color in this figure legend, the reader is referred to the web version of this article).

and the product turned into a hollow Cu microcage (as shown in Fig. S1b). Then, $AgNO_3$ aqueous solution was injected into the solution of hollow Cu microcages without using any surfactant under magnetic stirring. During this process, Ag^+ ions assembled on the surface of Cu nanoparticles, and then were reduced into Ag atoms and continually assembled into small Ag sheets (as shown in Fig. S1c). Lastly, with smaller Ag nanosheets growing epitaxially and becoming concave, bigger Ag NSs with smooth surface were produced until all the Cu nanoparticles were consumed (as shown in Fig. S1d).

The as-prepared Ag NSs were firstly characterized by SEM observations. Fig. 1a and b show the holistic and representative images of Ag NSs. It can be seen that the as-prepared products mainly consisted of ultrathin sheets having varying breadth, which lied in the range from 1 to 10 μm. Most of the Ag NSs displayed good dispersibility and uniformity, and they appeared curly with smooth surfaces. Moreover, from the high-magnification FESEM image (Fig. 1c), it can be clearly seen that the typical thickness of single Ag nanosheet was about 10 nm, which exhibited a high specific surface area due to its relatively low thickness and huge size. The NSs were further observed through the transmission electron microscopy (TEM) (as shown in Fig. 1d-f). As shown in Fig. 1e, the lattice spacing was 0.204 nm, which was in good agreement with the (2 0 0) lattice spacing of Ag. The selected area electron diffraction (SAED) pattern (Fig. 1f) indicated that the monocrystalline feature of the nanosheets. The interplanar spacings can be attributed to the $(\bar{2}\ 0\ \bar{2})$, $(0\ 2\ \bar{2})$ and (2 2 0) planes of Ag, respectively. HAADF-STEM presents a brighter contrast on the edges and in the center of sheet (Fig. 1g), suggesting that the surface was curved. The corresponding composition was confirmed by EDS mapping (Fig. 1h-j). Additionally, Ag (green color) was distributed in the whole zone of the nanosheet, whereas little residual Cu (red color) was observed (less than 5%, see Fig. S2), which was unavoidable during the galvanic replacement reaction.

The crystalline phase of the Ag NSs was characterized by XRD (as shown in Fig. S3a). According to the standard monoclinic structure of Ag crystal (JCPDS no. 0783), all the diffraction peaks can be indexed to (1 1 1), (2 0 0) and (2 2 0) planes of crystalline Ag, which were in good

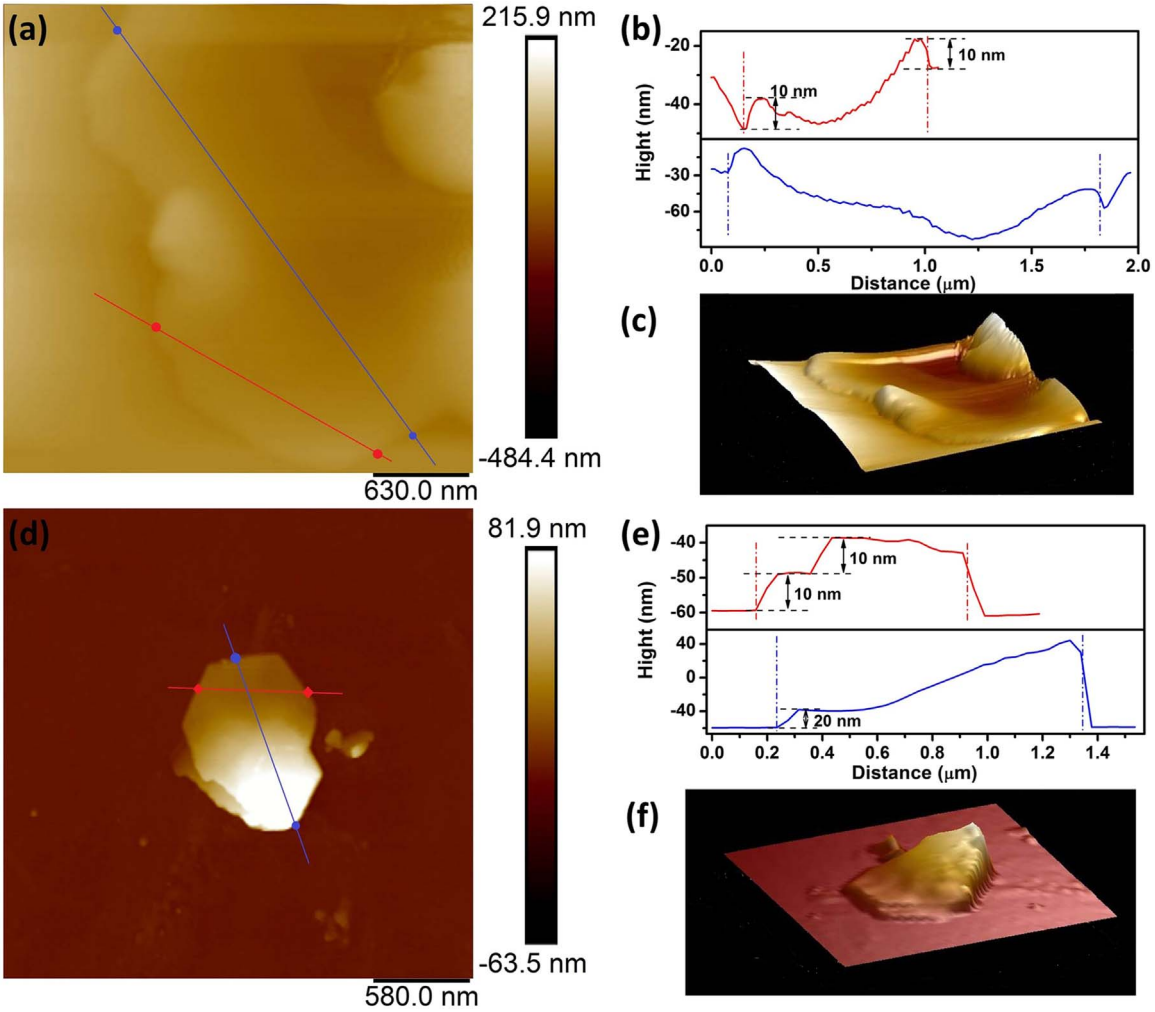

Fig. 2. (a) AFM image of single layer Ag nanosheet. (b) Height profile of the image in (a). (c) 3D image of single layer of Ag nanosheet in (a). (d) AFM image of double layers Ag NSs. (e) Height profile of the image in (d). (f) 3D image of double layer Ag NSs in (d).

agreement with the above results from SAED analysis. In addition, no peaks of other impurities including Cu crystals were detected. XPS was also applied to investigate the composition of Ag NSs. The full spectrum analysis result is shown in Fig. S3b, suggesting that except for C and O elements (from the atmosphere), Ag element was comfortably detected, whereas very weak peaks of Cu element were also observed. As shown in Fig. S3c, the peaks located at the binding energies of 968.2 eV and 974.2 eV were assigned to Ag $3d_{5/2}$ and Ag $3d_{3/2}$ in zero valence state, respectively. Meanwhile, the inconspicuous existence of peaks at higher binding energy of around 933 eV confirmed that vary little quantity of Cu existence in the Ag NSs (Fig. S3d).

Furthermore, in order to investigate and characterize the topography of Ag NSs, AFM was employed, which is the most direct method to quantify the thickness of nanosheets. The heights of two pieces of Ag NSs were measured, and the typical AFM image is shown in Fig. 2. One piece was a single nanosheet (Fig. 2a), while the other one consisted of two nanosheets stacked on each other (Fig. 2d). The height of edge (Fig. 2b,c) indicated a uniform thickness of about 10 nm, while the surface breadth was found to be up to several micrometers. These results further confirmed that the Ag NSs had nano-scale thickness. Furthermore, the results from height measurement confirmed a curved and bowl-shaped surface. All these results agree well with the above results obtained from the SEM.

3.2. Construction of Ag NSs-based H_2O_2 sensor

In order to identify the application of the synthesized Ag NSs, an enzymeless H_2O_2 sensor was fabricated using the Ag NSs. Fig. 3a shows the cyclic voltammograms (CVs) of the bare GCE and Ag NSs/GCE in 0.1 M PBS (pH 7.4) in the absence and presence of 5 mM H_2O_2 at a scan rate of 100 mV/s. In comparison with the CV response without H_2O_2, a remarkable reduction peak was found at −0.64 V (versus Ag/AgCl) with the responsive current of about 330 μA for Ag NSs/GCE. To confirm if the catalysis activity was mainly from the Ag NSs, a control experiment was carried out on the bare GCE. The results indicate that the response of the GCE towards the reduction of H_2O_2 was negligible compared with that of the Ag NSs/GCE. Besides, the active surface area of the electrode was determined by CV. Fig. S4 shows the well-defined redox peaks (ΔEp = 170 mV), indicating a quasi-reversible reaction (Wang, 2006), and the active surface area of Ag NSs/GCE was calculated to be 0.22 cm^2 (the geometric surface area of bare GCE is 0.196 cm^2), indicating an additional electroactive sites for electron transfer.

Moreover, to verify the sensitivity of Ag NSs/GCE towards the reduction of H_2O_2, the CVs were measured in different H_2O_2 concentrations with the successive addition of 0.5 mM H_2O_2, Fig. 3b shows the CV of the AgNSs/GCE with increasing the concentration of H_2O_2 from 0.5 mM to 3.0 mM. It was found that the responsive current of H_2O_2 increased with the increasing of concentration. These results clearly suggest that the Ag NSs possess excellent catalysis activity towards the

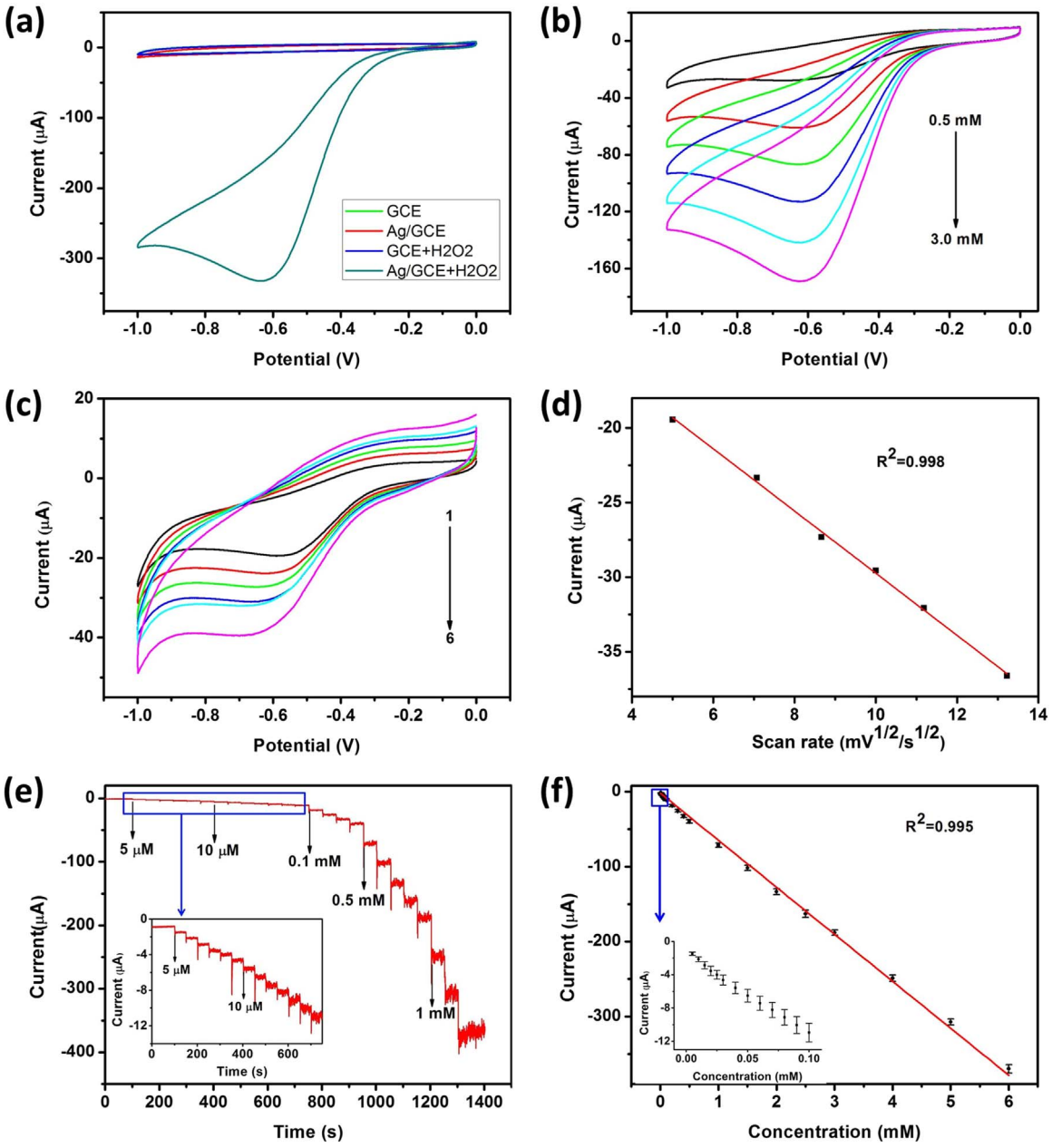

Fig. 3. (a) CVs of GCE and Ag NSs/GCE electrodes in N_2-saturated 0.1 M PBS solution containing 5 mM H_2O_2 and without H_2O_2, at a scan rate of 100 mV/s. (b) CVs in N_2-saturated 0.1 M PBS in the absence and presence of H_2O_2 with different concentrations (0.5, 1, 1.5, 2, 2.5, 3 mM), at a scan rate of 100 mV/s. (c) CVs in N_2-saturated 0.1 M PBS containing 0.5 mM H_2O_2 at different scan rates (25, 50, 75, 100, 175 mV/s). (d) Relationship between the electrocatalytic peak current vs square root of scan rate. (e) Amperometric responses to the successive addition of H_2O_2 in PBS at an applied potential of −0.5 V. The inset shows a close look of the blue oval region with the H_2O_2 concentration ranging from 5 to 100 μM. (f) The dependence of the response of electrodes on H_2O_2 concentration. The inset shows a closer look of the blue oval region with the H_2O_2 concentration from 5 to 100 μM.

reduction of H_2O_2. Furthermore, when plotting the peak of reduction current (Fig. S5), a decent linear relationship was obtained, indicating fairly good response as well. Besides, the CVs of the Ag NSs/GCE at different scan rates (25, 50, 75, 100, 125, and 175 mV/s) were investigated. As shown in Fig. 3c, the current of reduction peak increased with the increasing of scan rate. When the scan rate was in the range of 25–175 mV/s, the reduction peak increased linearly with the square root of scan rate, and the correlation coefficient was 0.998 (Fig. 3d), indicating fast electron transfer kinetics on Ag NSs/GCE and a typical diffusion-controlled process.

Before researching the typical amperometric response for H_2O_2, suitable measures should be taken to determine the optimum potential. The amperometric response under different potentials (from −0.7 to −0.4 V vs Ag/AgCl) was recorded with the successive additions of 1 mM H_2O_2. Compared with the potential of −0.6 V and −0.7 V, the response current of −0.5 V was the most stable and had very small background noise (Fig. S6a). Through calibration curves for the current-concentration correlation, the linear relationship was observed over a wide range of available potentials (Fig. S6b). Therefore, a typical potential of −0.5 V was chosen as the optimum potential of H_2O_2 sensing after considering the sensitivity, linear relationship and the stability of current.

The current-time measurements were undertaken to evaluate the sensitivity of Ag NSs/GCE for H_2O_2 detection at the potential of −0.5 V (Fig. 3e). The results indicate that, with the injection of H_2O_2 in the wide range of 5 μM to 6 mM, the current steadily increased as well. Meanwhile, the current response increased extremely rapidly with the change of H_2O_2 concentration, and reached a steady state within 2 s

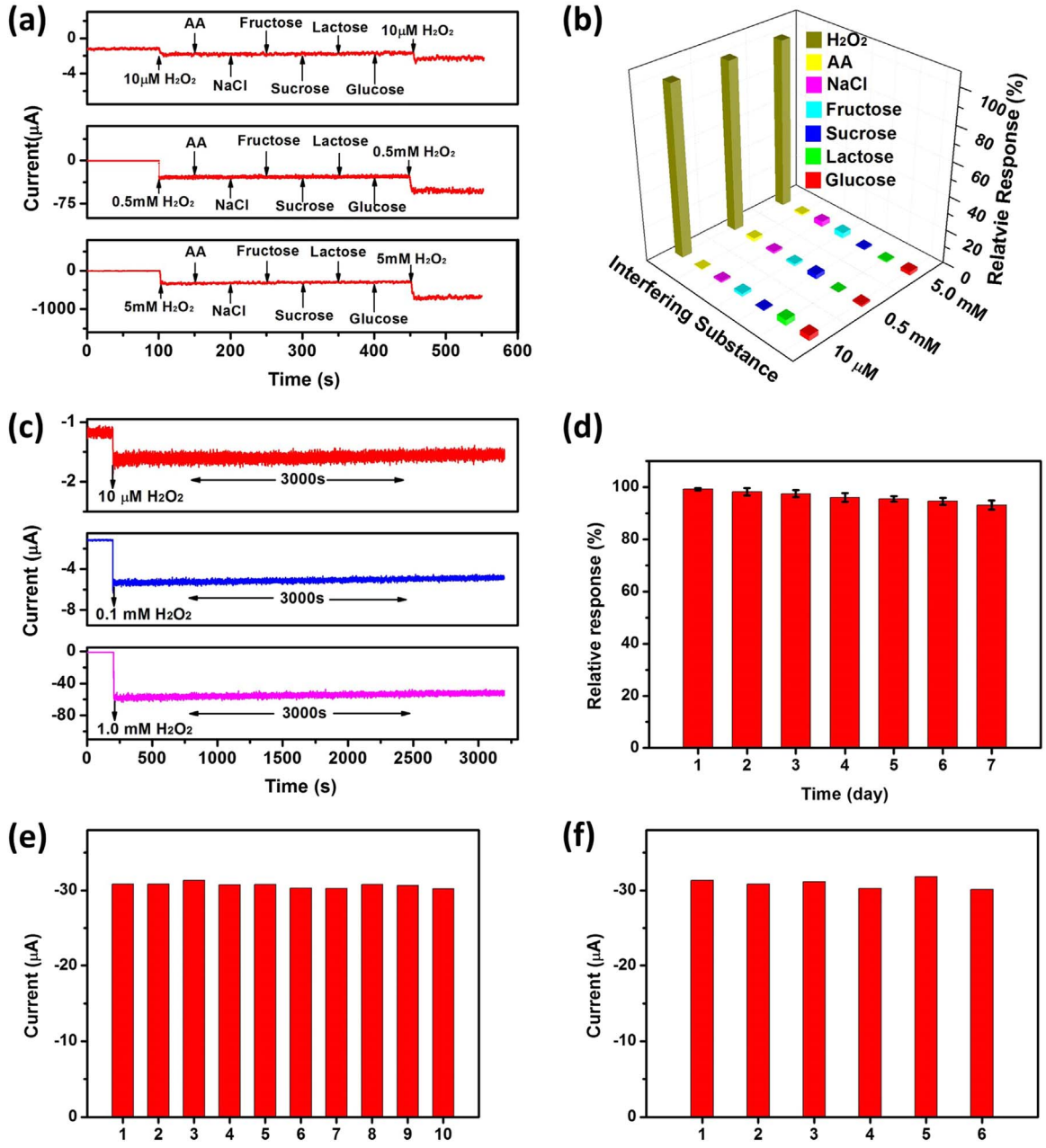

Fig. 4. (a) Chronoamperometric curves of the Ag NSs/GCE in response to the successive addition of 5 mM AA, NaCl, fructose, sucrose, lactose, and glucose with different H_2O_2 concentration (10 μM, 0.5 mM and 5 mM) in PBS at a constant potential of −0.5 V. (b) Histogram of the selectivity to various interfering substances. (c) Time-dependent current in 10 μM, 0.5 mM and 5 mM H_2O_2. (d) Stability test over 7 days in the air at room temperature. (e) The current response of 10 repeated amperometric measurements using the same AgNSs/GCE in PBS containing 0.5 mM H_2O_2. (f) The current response of 6 different AgNSs/GCEs prepared under the same conditions in PBS containing 0.5 mM H_2O_2.

after each addition, thus suggesting a rapid absorption and electrochemical activation of H_2O_2 molecules on the surface of Ag NSs/GCE electrode (Fig. S7). The linear relationship between the current and H_2O_2 concentration (Fig. 3f) exhibited a wide linear range of 5 μM to 6 mM with a correlation coefficient of 0.995. More importantly, the detection has a high sensitivity of about 320.3 uA mM^{-1} cm^{-2} calculated by k/s, where k and s are the slope of the calibration curve of amperometric results and the area of electrode, and a low detection limit of 0.17 μM estimated by $3\sigma/k$, where σ is the standard deviation of the background current. In comparison to other reports related to noble metal-based electrochemical sensors, the sensitivity was relatively higher and the detection limit of H_2O_2 was significantly lower (see Table S1). Furthermore, to verify the lowest detectable limit, the current response was tested for the H_2O_2 concentration within the range of 0.2–1.0 μM. And in the narrow range, it has an extremely high sensitivity of about 1680 uA mM^{-1} cm^{-2}. The result showed that H_2O_2 with very low concentration could effectively be detected and the corresponding calibration curve showed a correlation coefficient of 0.996 (Fig. S8).

Meanwhile, more comparison and analysis were shown in Table S2. Firstly, we compared the electrocatalytic activity of 26-facet Cu_2O crystals (Fig. S9) and hollow Cu microcages (Fig. S10) modified GCE. It can be seen that Ag NSs/GCE shows evident advantages compared to 26-facet Cu_2O/GCE and hollow Cu/GCE, including the detection limit, the sensitivity and the stability. Secondly, by changing the amount of $AgNO_3$, we investigated the electrochemical behaviors of various contents of Cu impurity (44.94% and 22.35%) in the Ag NSs (Figs. S11 and S12). With the decrease of Cu impurity, the detection limits grow lower and the sensitivities become higher, indicating that Ag is decisively favorable and Cu impurity is negative for the detection of H_2O_2.

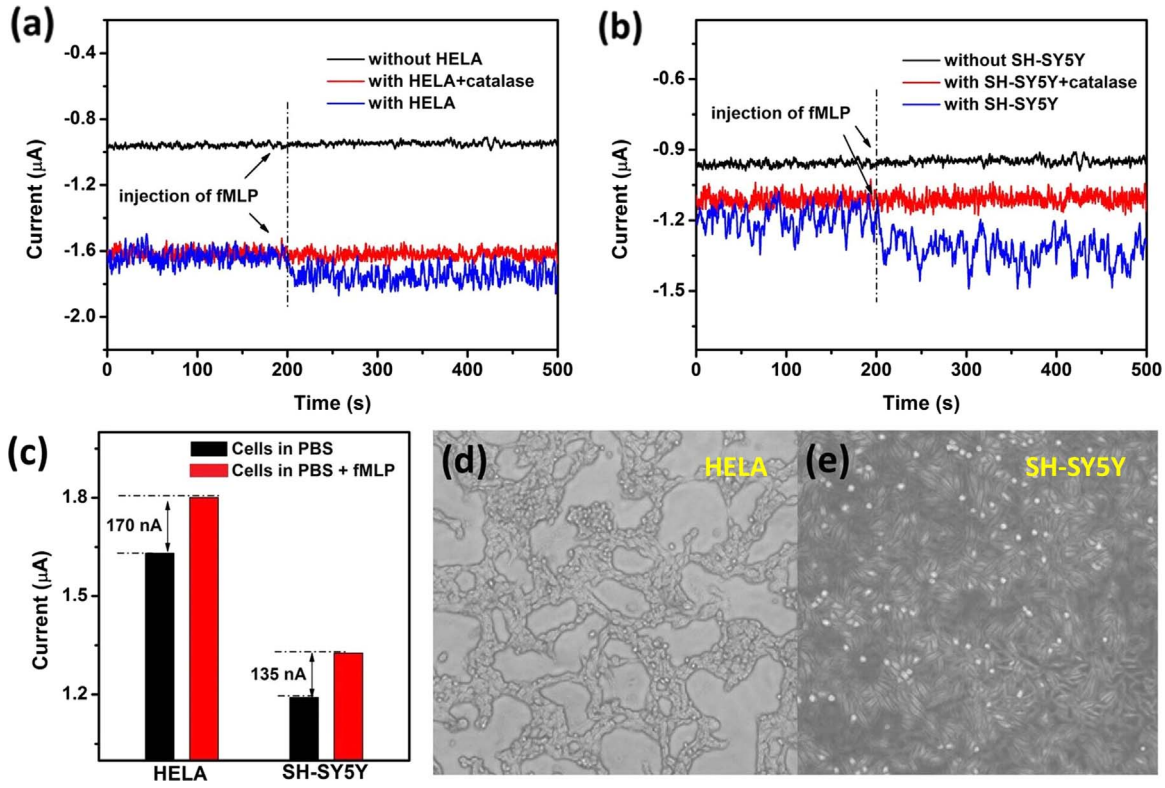

Fig. 5. (a) Amperometric responses of the Ag NSs/GCE to the addition of fMLP without HELA cells, with HELA cells, and with HELA cells and catalase in the N_2 saturated PBS at −0.5 V vs Ag/AgCl, respectively. (b) Amperometric responses to the addition of fMLP without SH-SY5Y cells, with SH-SY5Y cells, and with SH-SY5Y cells and catalase in the N_2 saturated PBS at −0.5 V vs Ag/AgCl, respectively. (c) Comparing the catalytic current response of the H_2O_2 released from HELA and SH-SY5Y cells. (d) Bright-feld microscopy image of Hela cells. (e) Bright-feld microscopy image of SH-SY5Y cells.

Thirdly, in order to strengthen the enhanced electrocatalysis activity of Ag NSs, we studied the electrochemical behaviors of Ag nanoparticles (NPs) and Ag nanowires (NWs) (Figs. S13 and S14). Compared with 0-D Ag NPs and 1-D NWs, the ultrathin 2-D Ag NSs exhibit higher specific surface area and more active sites, showing enhanced electrochemical performance.

3.3. Selectivity, stability and reproducibility of the constructed H_2O_2 sensor

Since Ag shows catalytic behavior towards many materials, which is associated with the practical application, therefore a confirmation of selectivity of sensors for H_2O_2 detection should be researched. As shown in Fig. 4a,b, the selectivity of the sensor was investigated by adding of several potential interfering substances (5 mM), including AA, NaCl, fructose, sucrose, lactose, and glucose. The results showed regardless of the concentration of H_2O_2 (10 μM, 0.5 mM and 5 mM), and all the interfering substances only caused negligible current response for the detection of H_2O_2, indicating the high catalytic selectivity of Ag NSs toward H_2O_2 detection. Besides, the stability of Ag NSs/GCE was also investigated by recording the amperometric response over a period of 3000 s in PBS at different H_2O_2 concentration (10 μM, 0.1 mM and 1.0 mM). As shown in Fig. 4c, after 3000 s, the reduction current retained 96.02% (for 10 μM), 92.42% (for 0.1 mM), and 90.89% (for 5 mM) of its initial value, respectively, suggesting that there was no obvious inhibitory effect on the Ag NSs/GCE response to its reduction current of H_2O_2. Moreover, the long-term storage stability of Ag NSs/GCE was also tested by investigating the current response of H_2O_2 on daily basis. As shown in Fig. 4d, after seven days in the air at room temperature, the original response was still maintained about 93.10% of its original level. All the results suggest a superior long-term stability of the Ag NSs sensor. Moreover, the reproducibility of the single Ag NSs/GCE toward H_2O_2 was investigated by recording the current response of ten repeated amperometric measurements in PBS. The calculated relative standard deviation (RSD) of the reduction current of 0.5 mM H_2O_2 was 1.1% for 10 successive measurements (Fig. 4e), indicating low susceptibility to electrode fouling. On the other hand, the RSD of electrode-to-electrode reproducibility (n = 6) was also investigated by using the solution of 0.5 mM H_2O_2 (Fig. 4f). And the calculated RSD was 2.1%, suggesting that the fabrication method of Ag NSs/GCE was extraordinarily reproducible.

3.4. The living cancer cell detection

As one of the most important molecular product related to a number of in vivo cell functions, H_2O_2 has been recently reported as a potential marker for some tumor cells (Li et al., 2016). Consequently, the Ag NSs/GCE were used to detect H_2O_2 released from some living cancer cells, including HeLa cells and SH-SY5Y cells (Fig. 5d,e). Additionally, N-formylmethionyl-leucyl-phenylalanine (fMLP) was used the stimulating agent, and induced the generation of H_2O_2 from living tumor cells in a short period of time (Maji et al., 2014). The two cancer cells were cultivated separately, and tested with the same electrochemical cell described above, which used the amperometric technique in 0.1 M PBS at the optimum potential of −0.5 V. As shown in Fig. 5a-b, the response current (black line) did not change without cells when 0.5 μM fMLP was added into PBS. However, with the addition of 0.5 μM fMLP into PBS with HELA and SH-SY5Y cells, the recorded current (blue line) increased obviously. In contrast, no obvious change in current (red line) was observed in the presence of catalase after the addition of 0.5 μM fMLP, confirming that the detective H_2O_2 was induced only from the living cells and the abnormal growth of tumor enhanced the production of H_2O_2. Moreover, as shown in Fig. 5c, the current signal changed following a different pattern for HeLa cells and SH-SY5Y cells. The current values were found to be 170 nA (for HELA) and 135 nA (SH-

SY5Y), which corresponded to 0.52 μM and 0.41 μM H_2O_2 generated from the cells, respectively. And this agrees well with the present electrochemical sensor of H_2O_2 from HELA cells (Ju and Chen, 2015; Liu et al., 2015). These results are of great significance for the application of therapeutic strategies and cancer chemoprevention.

4. Conclusions

In conclusion, ultrathin concave Ag NSs were successfully synthesized and the modified electrodes displayed excellent performance for the detection of H_2O_2. Besides, the practical workability was confirmed by the detection of H_2O_2 from living cancer cells. In addition, the Ag NSs-based sensors and devices in extensive applications should be evaluated in the future.

Acknowledgements

This work was supported by National Natural Science Foundation of China (NSFC no. 51501140), Shaanxi Province Science Foundation for Youth (no. 2016JQ5028), China Postdoctoral Science Foundation (2016M602808), Natural Science Foundation of Jiangsu Province (BK20161250, BK20171235), Public Welfare Technology Application Research Project of Zhejiang Province (2016C31G4181807) and the Fundamental Research Funds for the Central Universities (C.C. Kong and Q. Huang).

Appendix A. Supporting information

Supplementary data associated with this article can be found in the online version at http://dx.doi.org/10.1016/j.bios.2018.01.041.

References

Bai, J., Jiang, X., 2013. Anal. Chem. 85, 8095–8101.
Bai, Z., Li, G., Liang, J., Su, J., Zhang, Y., Chen, H., Huang, Y., Sui, W., Zhao, Y., 2016. Biosens. Bioelectron. 82, 185–194.
Chen, S., Hai, X., Chen, X.-W., Wang, J.-H., 2014. Anal. Chem. 86, 6689–6694.
Chhowalla, M., Shin, H.S., Eda, G., Li, L.J., Loh, K.P., Zhang, H., 2013. Nat. Chem. 5, 263–275.
Dai, H., Lü, W., Zuo, X., Zhu, Q., Pan, C., Niu, X., Liu, J., Chen, H., Chen, X., 2017. Biosens. Bioelectron. 95, 131–137.
Dong, C., Zhong, H., Kou, T., Frenzel, J., Eggeler, G., Zhang, Z., 2015. ACS Appl. Mater. Interfaces 7, 20215–20223.
Elzanowska, H., Abu-Irhayem, E., Skrzynecka, B., Birss, V.I., 2004. Electroanalysis 16, 478–490.
Ferri, T., Poscia, A., Santucci, R., 1998. Bioelectrochem. Bioenerg. 45, 221–226.
Gao, T., Wang, Y., Wang, K., Zhang, X., Dui, J., Li, G., Lou, S., Zhou, S., 2013. ACS Appl. Mater. Interfaces 5, 7308–7314.
Ge, S., Liu, W., Liu, H., Liu, F., Yu, J., Yan, M., Huang, J., 2015. Biosens. Bioelectron. 71, 456–462.
Giorgio, M., Trinei, M., Migliaccio, E., Pelicci, P.G., 2007. Nat. Rev. Mol. Cell Biol. 8, 722–728.
Guo, C., Hu, F., Li, C.M., Shen, P.K., 2008. Biosens. Bioelectron. 24, 819–824.
He, P., Liu, H., Li, Z., Liu, Y., Xu, X., Li, J., 2004. Langmuir 20, 10260–10267.
Jang, E., Kim, S., Koh, W.-G., 2012. Biosens. Bioelectron. 31, 529–536.
Ju, J., Chen, W., 2015. Anal. Chem. 87, 1903–1910.
Jv, Y., Li, B., Cao, R., 2010. Chem. Commun. 46, 8017–8019.
Karimipour, M., Razavi, F.S., Molaei, M., 2017. Plasmonics.
Kim, G., Lee, Y.-E.K., Xu, H., Philbert, M.A., Kopelman, R., 2010. Anal. Chem. 82, 2165–2169.
Kong, C., Sun, S., Zhang, X., Song, X., Yang, Z., 2013. CrystEngComm 15, 6136.
Lambeth, J.D., 2004. Nat. Rev. Immunol. 4, 181–189.
Lee, C.-Y., Zhao, Y., Wang, C., Mitchell, D.R.G., Wallace, G.G., 2017. Sustain. Energy Fuels 1, 1023–1027.
Li, Z., Meng, G., Liang, T., Zhang, Z., Zhu, X., 2013. Appl. Surf. Sci. 264, 383–390.
Li, Z., Xin, Y., Wu, W., Fu, B., Zhang, Z., 2016. Anal. Chem. 88, 7724–7729.
Liang, L., Lan, F., Li, L., Su, M., Ge, S., Yu, J., Liu, H., Yan, M., 2016. Biosens. Bioelectron. 82, 204–211.
Liu, J., Bo, X., Zhao, Z., Guo, L., 2015. Biosens. Bioelectron. 74, 71–77.
Maji, S.K., Sreejith, S., Mandal, A.K., Ma, X., Zhao, Y., 2014. ACS Appl. Mater. Interfaces 6, 13648–13656.
Mazeiko, V., Kausaite-Minkstimiene, A., Ramanaviciene, A., Balevicius, Z., Ramanavicius, A., 2013. Sens. Actuators B: Chem. 189, 187–193.
Miller, E.W., Albers, A.E., Pralle, A., Isacoff, E.Y., Chang, C.J., 2005. J. Am. Chem. Soc. 127, 16652–16659.
Shukla, V.K., Yadav, P., Yadav, R.S., Mishra, P., Pandey, A.C., 2012. Nanoscale 4, 3886–3893.
Sun, S., Song, X., Kong, C., Liang, S., Ding, B., Yang, Z., 2011. CrystEngComm 13, 6200.
Tajabadi, M.T., Basirun, W.J., Lorestani, F., Zakaria, R., Baradaran, S., Amin, Y.M., Mahmoudian, M.R., Rezayi, M., Sookhakian, M., 2015. Electrochim. Acta 151, 126–133.
Tsaplev, Y.B., 2012. J. Anal. Chem. 67, 506–514.
Wang, J., 2006. Analytical Electrochemistry, 3rd ed. John Wiley & Son Inc, New Jersey.
Wang, J., Musameh, M., Lin, Y., 2003. J. Am. Chem. Soc. 125, 2408–2409.
Wang, N., Cao, X., Chen, Q., Lin, G., 2012. Chemistry 18, 6049–6054.
Wang, T., Zhu, H., Zhuo, J., Zhu, Z., Papakonstantinou, P., Lubarsky, G., Lin, J., Li, M., 2013a. Anal. Chem. 85, 10289–10295.
Wang, Y., Yang, X., Bai, J., Jiang, X., Fan, G., 2013b. Biosens. Bioelectron. 43, 180–185.
Zhou, J., Liao, C., Zhang, L., Wang, Q., Tian, Y., 2014. Anal. Chem. 86, 4395–4401.